Dyads of G-Quadruplex Ligands Triggering DNA Damage Response and Tumour Cell Growth Inhibition at Subnanomolar Concentration

G-quadruplex dyad ligands triggering DNA damage response and tumour cell growth inhibition at sub-nM concentration

Doria, Filippo;[a] Salvati, Erica; [b,c] Pompili, Luca;[b] Pirota, Valentina;[a] Manoli, Francesco;[d] Nadai Matteo; [e] Richter Sara N.; [e] Biroccio, Annamaria;[b] Manet, Ilse;*[d] Freccero, Mauro*[a]

Abstract: Naphthalene diimide dyads exhibiting a different substitution pattern and linker length have been synthesized and evaluated as G-quadruplex (G4) ligands, investigating their cytotoxicity in selected cell lines. The dyads with the long C_7-linker exhibit extremely low IC_{50} values, below 10 nM, on different cancer cell lines. Contrary, the dyads with shorter C_4-linker were much less effective, with IC values increasing up to 1 μM. Among the three dyads with the longest linker, small differences in IC_{50} emerge, suggesting that its length plays a more important role rather than the substitution pattern. We have further shown that the dyads are able to induce cellular DNA damage response, which is not limited to the telomeric regions and is likely the origin of their cytotoxicity. Both absorption titrations and dynamic light scattering of the most cytotoxic dyads in the presence of hTel22 highlight their ability to induce effective G4 aggregation, acting as non-covalent cross-linking agents.

Introduction

DNA can adopt a variety of conformations apart from B-DNA.[1] These secondary conformations, include G-quadruplex structures (G4s), which consist of at least two or more *π-π* stacked planes of four guanosines cyclically bound to each other by hydrogen bonding according to the Hoogsteen motif.[2] Different G4 topologies exist in solution and likely also *in vivo*, depending on the sequence of the guanine(G)-rich oligonucleotide, the nature as well as the number of the loop nucleotides connecting the guanine(G)-rich tracts.[2b]
G-rich sequences are present in some very important regions of the human genome.[3] The extreme 3'-ends of telomeres consist of single-stranded (*ss*) oligonucleotides characterized by the repeating G-rich motif TTAGGG, shortening during DNA replication to protect chromosome genetic information.[4] Computational and biological data have shown that G-rich sequences are also frequent in other parts of the genome.[3b, 3c, 5] By means of high-throughput sequencing Balasubramanian et al. have mapped DNA G4 in the human genome, discovering new non-canonical long loop and bulged G4s.[6] During the last decade increasing evidence has also been obtained for the formation of G4s in RNA, especially in UTR regions.[7] All this has strengthened the hypothesis of implication of the G4s in regulatory processes like DNA transcription and RNA translation of vital importance for cell survival. The understanding of the biological importance of the G4 *in vivo* is still a matter of large debate.[8] By means of the development of a specific antibody directed against telomeric G4 the G4 structure has first been discovered *in vivo* at ciliate telomeres.[9] Next, two research groups independently reported the use of G4-specific antibodies that bind with nM affinity to visualize these structures in cells by means of fluorescence-based imaging.[10] They managed to visualize G4s at distinct locations on chromosomes, demonstrating changes in their frequency at different points in the cell cycle and an increase in their frequency in the presence of a small G4 ligand. These data are very persuasive of the G4 existence, biological significance, and potential "*drugability*" in human cells. In parallel, large amounts of data have been collected showing that small molecules stabilizing the G4s of a G-rich sequence are able to interfere with the biological processes involving the latter sequence.[11], [12]
In this frame, our interest goes to G4 binding naphthalene diimides (**NDIs**) which are extremely versatile compounds.[13] In fact, their optoelectronic properties can be effectively tuned by substituents on the aromatic core,[14] thus giving origin to absorption and emission in the red spectroscopic window, which makes them appealing for fluorescence imaging and photodynamic therapy (PDT). [15], [16] Additionally, NDIs have been exploited as appealing scaffold for the design of G4 ligands, thanks to their chemical accessibility and large planar surface. We and others have shown that tri-, tetra-substituted and core-extended NDIs are potent and reversible ligands [14c, 17] as well as alkylating agents targeting G-rich nucleic acids (NAs) folded into G4s.[18] In particular, Neidle et al. reported a series of NDIs, with side-chains composed of 3-5 carbons linking a positively charged methyl-piperazine functionality to the NDI core, that significantly stabilize human telomeric G4 DNA and inhibit the growth of several cancer cell lines at sub-μM concentrations.[17a, 19] Some inhibited the telomerase complex in accord with the hypothesis that these NDIs act at the cellular level through telomeric G4 stabilization. They also showed significant antitumor activity associated with telomerase inhibition in a xenograft model for pancreatic cancer.[20] More recently, we have published a series of NDIs (**1**-**4**, Scheme 1) having excellent water solubility and cellular entry, merged with promising features for theranostic applications. [15-16] In particular the tetra-substituted compound **4** was able to produce singlet oxygen, and induced photo-cytotoxicity.[16] Nuclear uptake was evidenced by fluorescence confocal imaging exploiting the

[a] Dr. F. Doria, Dr. V. Pirota, Prof. M. Freccero
Department of Chemistry, University of Pavia, V. le Taramelli 10, 27100 Pavia, Italy
E-mail: mauro.freccero@unipv.it
[b] Dr. E. Salvati, L. Pompili, Dr. A. Biroccio
Oncogenomic and Epigenetic Unit, IRCCS Regina Elena National Cancer Institute, Via Elio Chianesi, 53 00144 Rome, Italy
[c] Dr. E. Salvati. Present address: Istitute of Molecular Biology and Pathology (IBPM) National Research Council (CNR), Via degli Apuli, 4 00185 Rome, Italy
[d] F. Manoli, Dr. I. Manet
Institute for Organic Synthesis and Photoreactivity (ISOF), National Research Council (CNR), via P. Gobetti 101, 40129 Bologna Italy
E-mail: ilse.manet@isof.cnr.it
[e] Dr. M. Nadai, Prof. S. N. Richter
Department of Molecular Medicine, University of Padua, via Gabelli 63, 35121 Padua, Italy

Supporting information and the ORCID identification number(s) for the author(s) of this article can be found via a link at the end of the document.

intrinsic NDI fluorescence. We further explored this class of compounds producing the NDI dyad **5**, see Scheme 1.[21]

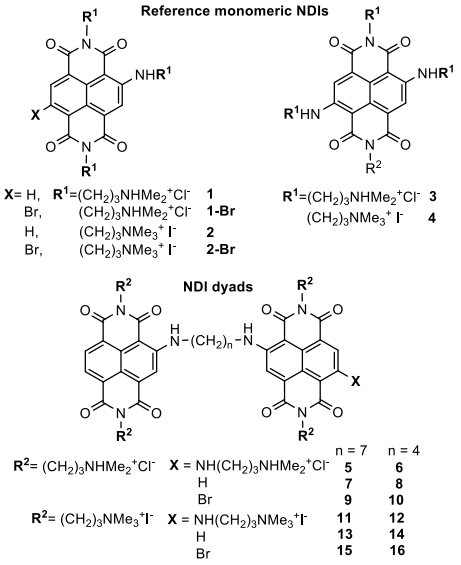

Scheme 1. NDI dyads synthesized and evaluated as G4 ligands (**5-16**) in comparison to the reference monomeric NDI units **1-4**.

This dyad has remarkably appealing optical properties for *in vivo* applications aiming at ligand/G4 interaction and detection. In fact, the non-fluorescent dyad **5**, conjugating a red and blue NDI dye, becomes red emitting upon G4 binding. Moreover, the average fluorescence lifetime is significantly different for the NDI-dyad/G4 and the dyad/dsDNA complexes, and can represent a key feature for the development of new rationally engineered G4 sensors.[21] Although, the binding affinity of **5** was good toward c-Myc (pK_{11} 5.9, with 1:1 stoichiometry) and hTel22 (pK_{21} 11.6, with a 2:1 ligand/G4 stoichiometry), we did not measure any significant cooperative effect of the two binding units.[21] In an attempt to improve both the binding and emission properties upon G4-binding we further explored compound **5** and eleven new NDI dyads. We modulated the spacer length using, apart from the heptyl linker, also a shorter butyl linker to tether the two NDIs. No polyethylglycol (PEG) linkers was included, as we have recently shown that they are unsuitable to implement both the binding and the sensing response of coumarin-NDI dyads (Ref: Ref: Zuffo, M.; Ladame, S.; Doria, F.; Freccero, M.* *Sensors and Actuators, B: Chemical* **2017**, *245*, 780-788). We varied the substituent X on the aromatic core to investigate the effect of the nature of the NDI comparing homo- dyads, where the NDI units are identical, with the hetero-dyads, exhibiting two different binding NDIs. Finally, we evaluated the importance of the overall charge of the dyad via quaternization of amines (**5-16**, Scheme 2). In this paper, we report (i) the synthesis of the new compounds (**6, 10-16**) and their characterization, (ii) the photophysical behaviour of the amines **5-10** and their quaternary ammonium salts **11-16** together with (iii) the binding potential towards G4 DNA and ds DNA for the most cytotoxic **5-9**. In fact, the solution study has been completed with cell studies highlighting unexpected low nM inhibitory concentration of **5**, **7** and **9** in tumour cell lines, combined with the activation of the DNA damage response (DDR) machinery.

Results and Discussion

Synthesis

2,6-dibromo-substituted NDI **17** is the common precursor to the ligands **1-16**. **17** has been synthesized according to a well-established procedure[22] and used for the next step (*a*) without further purification (Scheme 2). The subsequent nucleophilic aromatic substitution (S_NAr, step *a*) and the reductive debromination (*b*), were both carried out using a published procedure, which was optimized for 1,7-diaminoheptane, yielding **19** and **21** in good yields.[15-16] These NDIs are less reactive than **17** in a S_NAr, therefore we were forced to perform the following step *c*) under harsher conditions, by a microwave-assisted conditions in DMF as solvent (150°C, 200 psi, 200 W, in sealed reaction vessels), which allows us to reduce both the reaction time (20 min) and the by-products. The third microwave assisted S_NAr (step *d*) carried out in neat N^1,N^1-dimethylpropane-1,3-diamine gave the hetero-dyads **5** and **6** in 3 min, in quantitative yields. Subsequent HPLC preparative purification (CH_3CN: H_2O and 0.1% CF_3COOH as eluent), and final anion exchange, yielded **5-10** as hydrochloride salts. Exhaustive methylation of all the dyads gave the quaternary ammonium salts **11-16**.

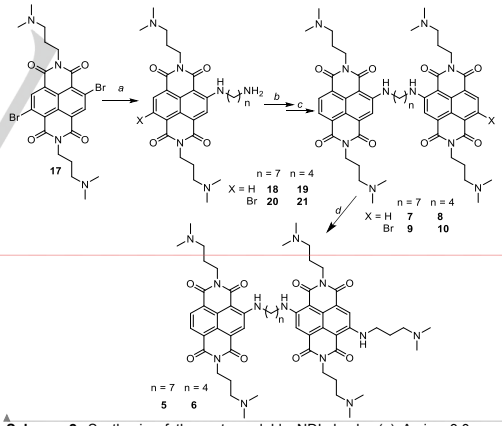

Scheme 2. Synthesis of the water soluble NDI dyads. (a) Amine 3.0 eq., CH_3CN, 75°C, 5 h (b) $Na_2S_2O_4$ 2 eq. in aqueous CH_3CN (1:1), r.t. 2 hr. (c) NDI **17** 0.95 eq., DMF, microwave assisted protocol, sealed reaction vessels (M.W.; 150°C, 200 psi, 200 W, 20 min). (d) Neat N^1,N^1-dimethylpropane-1,3-diamine, microwave assisted protocol, sealed reaction vessels (M.W.; 150°C, 200 psi, 200 W, 3 min).

Photophysical study of the dyads

The dyads all exhibit very good solubility both in water and phosphate buffer being soluble up to 0.1 mM. The absorption spectra of the dyads containing amine moieties (**5-10**, Scheme

Unknown
Codice campo modificato

Sara 6/9/y 14:00
Formattato: Apice

Unknown
Codice campo modificato

Sara 6/9/y 14:00
Formattato: Non Evidenziato

Mauro Freccero 6/5/y 12:46
Commenta [1]: Ho inserito questo paragrafo per dendere più incisiva la scelta di non usare PEG

Sara 6/9/y 14:00
Formattato: Non Evidenziato

Sara 6/9/y 14:00
Formattato: Non Evidenziato

ilse 26/3/y 16:56
Commenta [2]: Noi prepariamo soluzioni di 1-5e-4 M senza problemi, andare più su non serve né per noi né per i test biologici, per me può bastare questo.

Mauro Freccero 6/5/y 12:45
Commenta [3]: OK

1) in aqueous solutions, at different pH (Figure 1), exhibit two bands, one in the 300-400 nm range typical of the aromatic NDI core, and the other in the visible of comparable intensity, due to the presence of one or two amine substituents on the aromatic core. The spectra do not change with pH. Additionally, the amine dyad spectra are very similar to those of the quaternary ammonium salts **11-16** (ESI, Figure S1), so the protonation state of the terminal propyl amine groups does not influence the absorption spectra.[23] As underlined previously, the visible absorption arises from a charge transfer (CT) transition involving the aromatic amines.[14a, 24] Noticeably, the absorption spectra of the dyads **5**-**10** differ from the sum of the monomeric spectra (**1**, **1-Br** and **3**), suggesting interaction of the NDI units. The shape of the absorption spectra is apparently reflecting the amount of interaction of the two chromophores within the dyad. Comparing the absorption spectra of dyads **5-6** we observe an inversion of the relative intensities of the peak at 352 and 373 nm on one hand and 532 and 645 nm on the other hand.[21]

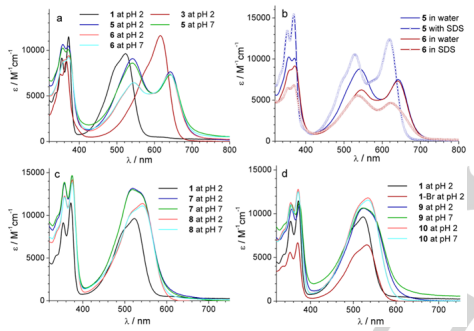

Figure 1. Absorption spectra of the dyads **5**-**10** (a, c and d) compared with the reference monomers **1**, **1**-Br and **3** in 10 mM Na^+ phosphate buffer of pH 2 and 7; (b) Absorption spectra of the dyads **5**-**6** with and without 35 mM SDS micelles in water; d=1 cm.

A similar effect is present in the visible absorption band of dyads **7-10** suggesting an active role played by the linker. Although, dilution experiments did not cause a significant change in the spectral shape, addition of sodium dodecyl sulfate (SDS) strongly influences the absorption spectra even though in opposite way for compounds **5** and **6**, favouring loss of interaction only for the former. The maxima shift to 625 and 525 nm for the two NDI units of dyad **5** in the presence of SDS, values close to the maxima of the monomer models, indicating that interaction between the two moieties within the dyad **5**, with the long linker, does not occur in the presence of SDS-micelles. Compared to the monomeric NDIs (**1**-**4**) the fluorescence quantum yield of the dyads at pH 2 is 10 to 100 times lower (Φ_F, Table 1).

A pH increase from 2 to 7 does not change Φ_F of the dyads **7**-**10**, while it causes a 40% reduction for the hetero-dyads **5** and **6**. The fluorescence lifetimes (τ_f) of the NDI dyads **5**-**10** do not vary with the pH so we are observing static quenching within the dyad. Noticeably, long lifetimes up to 10 ns are displayed by the dyads making their observation feasible in biological context generally exhibiting shorter lifetimes of 3-4 ns. As Φ_F improves only slightly comparing the quaternary ammonium salts with the respective amine compounds, intramolecular electron transfer (eT) involving dimethyamino groups plays a marginal role in the fluorescence quenching of the dyads. The intramolecular interaction of the two chromophores, suggested above on basis of the absorption spectra, likely accounts for additional non-radiative decay pathways of the excited states in the dyad. In this frame the shorter lifetimes and lower quantum yields of dyads **5-6** and **11-12** compared to dyads **7**-**10** and **13-16** can be reasonably explained by electron transfer from the electron-rich tetra-substituted NDI moiety to the electron poor one as additional quenching process. The double exponential decay of all dyads (τ_i, Table 1) cannot be trivially explained by the presence of two chromophores and likely the presence of dyads in different conformations and the relative orientation of the two NDI units may influence the various non-radiative deactivation processes and consequently the lifetime.

Table 1. Photophysical data of the compounds **5-10** in 10 mM Na^+ phosphate buffer at pH 2 and the compounds **11-16** in water (pH 7) together with the data of the reference monomers (**1-4**).

NDI	λ (nm)	ε ($M^{-1}cm^{-1}$)	Φ_F	τ / ns (f_i) [a]
1	522	9500	0.19	5.60 [b]
2	522	11000	0.21	5.50 [b]
3	616	11500	0.17	4.40 [b]
4	613	10700	0.17	4.00 [b]
5	642	7500	0.002	3.96 [c,d]
6	641	7300	0.002	1.40 (0.08), 5.10 (0.92) [c]
7	519	13100	0.008	3.21 (0.29), 9.19 (0.71) [b]
8	542	11400	0.013	3.26 (0.39), 8.88 (0.61) [b]
9	524	10650	0.011	3.06 (0.37), 9.19 (0.63) [b]
10	537	11800	0.028	3.52 (0.39), 10.59 (0.61) [b]
11	642	3200	0.003	3.13 (0.55), 5.16 (0.45) [c]
12	639	5200	0.005	3.40 (0.29), 4.79 (0.71) [c]
13	515	13000	0.021	3.05 (0.12), 9.42 (0.88) [b]
14	541	11100	0.048	3.37 (0.09), 9.31 (0.91) [b]
15	519	6300	0.023	3.00 (0.36), 9.39 (0.64) [b]
16	521	10550	0.033	3.27 (0.36), 9.44 (0.64) [b]

[a] Fluorescence lifetimes. For the double exponential decays, the population (f_i) is reported in parenthesis. [b] Excitation at 465 nm and τ measured at 610 nm. [c] Excitation at 637 nm and τ measured at 680 nm. [d] Decay also fits with bi-exponential function, 3.30 ns (47%) and 4.60 ns (53%).

FRET melting analysis of the new dyads as G4 ligands

We preliminary evaluated the binding of the NDI dyads **5**-**16** to G4 DNA by means of FRET melting experiments using the fluorescence-labelled human telomeric sequence F21T as a model for telomeric G4 DNA. We measured the melting temperatures (T_m) of F21T and dsDNA (ds26) by FRET in the absence and presence of the dyads in 100 mm K^+ solutions. The net T_m increment (ΔT) suggested that the dyads are all very good DNA binding ligands. However, the quaternary ammonium salts exhibited a poorer performance in terms of differentiation between G4 DNA and dsDNA, as three of them (**11**, **13** and **15**) stabilized dsDNA even more than G4 DNA (Figure 2).

Unknown
Codice campo modificato
Unknown
Codice campo modificato
Unknown
Codice campo modificato
Sara 6/9/y 14:00
Formattato: Tipo di carattere:Non
Sara 6/9/y 14:00
Formattato: Tipo di carattere:Non
Sara 6/9/y 14:00
Formattato: Tipo di carattere:Non
Sara 6/9/y 14:00
Formattato: Tipo di carattere:Non
Sara 6/9/y 14:00
Formattato: Tipo di carattere:Non
Grassetto
Sara 6/9/y 14:00
Formattato: Tipo di carattere:Non
Grassetto
Sara 6/9/y 14:00
Formattato: Non Evidenziato
Sara 6/9/y 14:00
Formattato: Non Evidenziato

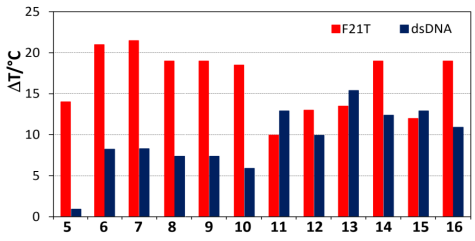

Figure 2. T_m increment (ΔT_m) of F21T (0.25 μM, red bars) and ds26 (blue bars) in the presence of the dyads **5**-**16** (1.0 μM) and 100 mM K^+ solution. Exc. 465 nm and emission at 510 nm.

The binding of dyads (i) **5,** the most G4 *vs* ds26 selective, (ii) **7,** the most stabilizing and (iii) **9,** a Br-containing dyad, to the F21T sequence was next competed by increasing concentrations of the unlabeled ds26 oligonucleotide (Figure 3).

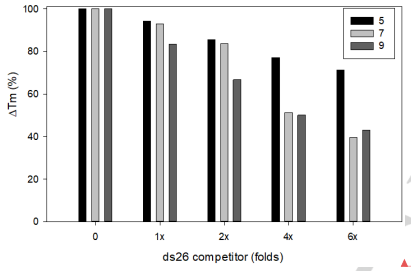

Figure 3. T_m increment (ΔT_m) of F21T (0.25 μM) in the presence of the dyads **5**, **7** and **9** (1 μM) and of unlabeled ds26 competitor (0-6x with respect to the F21T sequence), in 100 mM K^+ solution.

These G4-ligands retained up to 80% of the telomeric sequence stabilization in the presence of dsDNA. The least affected by the ds-competitor was the dyad **5**.

On the basis of the above FRET melting data, we decided to study the performance as G4 ligands and the biological activity toward tumour cell lines of different histological origin, only for the amine containing dyads (**5**-**10**), discarding the quaternary ammonium salts (**11**-**16**).

Biophysical assays of the dyads DNA binding performance. The complexation behaviour of dyads **5-9** towards four types of DNA has been studied by means of different spectroscopic techniques. In particular, we examined the binding to the hybrid G4 of a telomeric sequence (hTel22), the parallel G4 of G-rich sequences in the promoter regions of the c-myc (c-myc2345) and kras (kras) oncogenes and double stranded (ds) DNA of a self-complementary strand (ds26, see Table 3) as model of B-DNA. Titrations to monitor DNA binding consisted in the study of K^+ rich solutions of the compounds **5-9** at fixed concentration in the μM range with increasing amounts of DNA keeping the ligand excess below 6 and the DNA excess below 4. Absorption, fluorescence and circular dichroism (CD) spectra were recorded and fluorescence decays collected for all solutions.

Table 3. Oligonucleotides used in the present study.

NA	Sequence	Structure
ds26	5'-[CAATCGGATCGAATTCGATCCGATTG]-3'	ds DNA
hTel22	5'-A[GGGTTA]3GGG-3	hybrid G4
c-myc2345	5'-[GAGGGTGGG]$_2$GAAG-3'	parallel G4
kras	5'-[AGGGCGGTGTGGGAAGAGGGA]-3'	parallel G4

CD titrations. UV CD spectra show that dyads **5-9** bind to parallel G4 of c-myc2345 and kras, not significantly affecting their conformation as their CD spectra do not change in shape (Figure S2 binding to kras and c-myc2345). Differently, dyad binding favours transition from hTel22 hybrid G4 to other G4 structures (Figure S3). The length of the dyad linker seems more important than the nature of the NDI unit. At low DNA concentrations the negative ellipticity at 260 nm for compounds **5**, **7** and **9** may be indicative of partial transformation into antiparallel G4, while the more pronounced positive shoulder at 265 nm suggests a partial transition to a parallel G4 conformation for compounds **6** and **8** with the short linker. Dyad binding to ds DNA causes small changes of the CD in the UV as shown in Figure S2. CD in the visible attributable to the dyad due to complexation has been monitored (Figure S2), but in the case of G4 DNA no reliable signals were observed.

Absorption titrations. We can expect two effects contributing to changes in the absorption spectra. On one hand, disruption of the interaction between the two NDI units can occur causing an increase of the molar absorption coefficients both in the visible and the UV as well as a blue shift as shown by the effects of addition of SDS to a solution of compound **5**. On the other hand, interaction of the NDI units with the G4 or ds DNA platform can cause hypochromic effects as well as red shift of the maxima known to occur for NDI compounds interacting with DNA bases.[33] The changes observed in the absorption spectra (ESI, Figure S4) depend on the type of DNA. Maxima of the visible absorption peaks close to 640 and 540 nm confirm interaction of both NDI units of the dyads with the DNA. The absorbance peak at 640 nm of the hetero-dyads increases overall to a much greater extent compared to the 540 nm peak indicating that the tri-substituted NDI is mainly involved in the binding process. The significant increase of the absorbance in the visible in the presence of the hybrid hTel22 suggests the disruption of the intramolecular interaction of the two chromophores. In the case of parallel G4 DNA, the minimal changes of the shape of the visible absorbance band and the very limited increase of the absorbance are in line with stacking of at least one NDI unit, likely the tri-substituted NDI unit, with the G-tetrad without disrupting chromophore interaction. Differently, binding to ds DNA causes important hypochromicity for the UV band while absorbance increases up to 50% at the maxima in the visible for the dyads with the longer linker. Likely two effects, strongly reduced interaction of the two NDI units as well as intercalation,

most probably of the tri-substituted NDI unit, may occur in line with CD data. As final comment, we noted that especially in the case of binding of dyads with the longer heptyl linker the absorption spectra are affected by a baseline increasing in intensity toward the blue edge of the spectra. This may suggest that aggregation is occurring in solution. The effect has been further investigated and commented below.

Fluorescence titrations. Strikingly, the fluorescence of the compounds **7-9** is quenched while the fluorescence of both compounds **5** and **6** is turned on by DNA complexation to different extents and reaches fluorescence quantum yields of 4-5 %, a 25-fold increase with respect to the free dyads (Figure S5). Note that for dyads **5-6** only the moiety with four substituents becomes fluorescent, while the fluorescence of the tri-substituted unit is almost totally quenched. The former feature could be exploited to evidence the presence of the dimer **5** in cells (Figure S6). Complexation also reflects in the fluorescence decays. Global analysis required fitting with a tri-exponential function for dyads **7-9** (ESI Table S1): a new short lifetime of few hundreds of ps appears in the presence of DNA, the lifetime of ca 3 ns persists and the long lifetime component of ca 8 ns is losing weight with increasing DNA concentration. Global analysis converged with a triexponential decay function for dyads **5-6** in the presence of ds DNA and a 4-exponential decay function for G4 DNA. A complexed species with a longer lifetime than the free dyad exists for the dyad **5** with G4 DNA while the lifetime of ~ 5 ns of dyad **6** loses importance and a new lifetime of ca 3.8 ns appears (ESI Table 1). The multiple fluorescence lifetimes confirm the existence of different types of binding sites in the G4 topologies examined.

Analysis of absorption or fluorescence titration: evaluation of the binding constants and stoichiometry. Global analysis of the multi-wavelength data set corresponding to the absorption or fluorescence spectra of the different mixtures allowed to determine the best complexation model, the binding constants of the most stable complexes (Tables 3 and 4) as well as the individual absorption or fluorescence spectra of the associated species. Spectra of samples presenting increased absorption baseline were excluded from the analysis. In the case of parallel G4 (kras and c-myc2345) the complexation model consists overall in the existence of two complexed species with 1:1 and 1:2 (DNA:dyad) stoichiometry (with binding constants K_{11} and K_{12} respectively), while in the case of hTel22 and ds26 the analysis converged with a complexation model of one complex with 1:2 stoichiometry. Looking at the binding constants K_{11} (Table 4), **8** and **9** seem potent ligands for c-myc, unlike **7** and **5**. Data in Table 5 do not evidence important difference in affinity for the G4s in comparison to ds26.

Table 4. Binding constants obtained from multiwavelength global analysis of the fluorescence titration data yielding 1:1 stoichiometry complexes for parallel G4s (kras and c-myc2345). The calculated fluorescence quantum yields of the 1:1 complexes are indicated as Φ_F(kras) and Φ_F(cmyc).

Ligand	kras [a]	Φ_F(kras)	c-myc2345 [a]	Φ_F(cmyc)
5	6.8	0.036	5.9	0.042
6	6.7	0.055	6.5	0.069
7	6.8	<0.001	5.7	<0.001
8	7.7	<0.001	7.2	<0.001
9	6.8	<0.001	7.0	<0.001

[a] Binding constants as log K_{11}(M^{-1}).

Table 5. Binding constants obtained from multiwavelength global analysis of the fluorescence titration data yielding a 1:2 (DNA:ligand) stoichiometry complexes for hTel22 G4 compared to the logK_{12} (M^{-2}) towards kras and c-myc2345. The calculated fluorescence quantum yields of the hTel22-ligand complexes reported Φ_F(hTel22).

Ligand	hTel22 [a]	Φ_F(hTel22)	kras [a]	c-myc2345 [a]	ds26 [a]
5	11.7	0.044	13.2	12.7	11.7
6	12.0	0.040	13.3	13.2	12.8
7	12.9	<0.001	14.0	12.6	13.6
8	12.6	<0.001	13.3	13.5	12.1
9	13.0	<0.001	12.8	13.0	12.0

[a] Binding constants as log K_{12} (M^{-2}).

A closer look at the K_{12} binding constants (Table 5) suggests that **9** is the only dyad showing a modest hTel22/ds26 selectivity and **7** is the most potent ligand towards kras G4. The melting data above seem to suggest a slightly different selectivity trend, but we need to keep in mind that melting data only reflect the stability of the complex and not the affinity. On basis of the calculated fluorescence spectra of the complexed species, we obtained the fluorescence quantum yields of the complexes reported in Table 4 and 5. The dyads **7-9** have fluorescence quantum yield below 10^{-3} in all complexes independently of the stoichiometry and the G4 conformation as complexation causes quenching of the fluorescence. As to the dyads **5-6** only the 1:1 complex of parallel G4 exhibit a significantly increased fluorescence quantum yield, while in the case of hTel22 and ds26 the complex with 1:2 stoichiometry is fluorescent. The higher yields of **5** and **6** can be easily rationalized by the redox properties of the NDI units composing the dyads with the tetra-substituted being more electron rich and thus less easily reduced by electron transfer from the guanines.

In the case of parallel G4 we envisage at least two types of binding sites, that may involve stacking with the two tetrads, with one being thermodynamically more stable, and favoured in the case of excess parallel G4 resulting in a population of complexes with 1:1 stoichiometry. In the case of hybrid hTel22 it is hard to assess any binding site as complexation is changing the G4 conformation which gives obviously rise to multiple types of binding sites, necessary to settle the two dyads, that can consist in interaction with the grooves or loop nucleotides or tetrad stacking. This frame is in line with the observations on the global analysis of the fluorescence decays. For both the dyads **5** and **6** in the presence of G4 DNA excess, we discern up to 4

different lifetimes of the tetra-substituted unit attributable to at least 4 binding sites. Moreover, appearance of a fluorescence lifetime longer than that of the free dyad gaining importance with increasing DNA concentration is probably due to the tetra-substituted unit that may not be tightly bound to the DNA while the tri-substituted unit accounts for the DNA binding. In the case of the dyads **7-9**, the fit is possible with three lifetimes. Only one new lifetime emerges the short one, while the two longest lifetimes loose importance with increasing DNA concentration. In this case quenching by electron transfer is the dominating process, and the short lifetime can be found even in different binding sites while the long lifetimes likely belong to loosely bound NDI units.

Biological activity

Clonogenic assay. We investigated the cytotoxic effect of the NDI dyads in tumour cell lines of different histological origin (HCT116 and HT29, colorectal carcinoma; U2OS, osteosarcoma and MDA-MB231, breast carcinoma) by means of clonogenic assays, which allow measuring the capacity of cells to overcome a cytotoxic insult, by scoring their colony formation ability after drug exposure. All the NDI dyads resulted highly cytotoxic at sub-μM doses with different IC_{50} (Table 2 and Figure 4).

Table 2. IC_{50} and IC_{90} values of compounds in four different human cancer cell lines.

NDI	HCT116		HT29		U2OS		MDA-MB231	
	IC_{50}[a]	IC_{90}[a]	IC_{50}[a]	IC_{90}[a]	IC_{50}[a]	IC_{90}[a]	IC_{50}[a]	IC_{90}[a]
1	50	200	100	130	20	60	<10	>10
3	41.5	80	200	890	36	110	160	500
5	5.7	8.9	7.9	29	8.6	161	1.31	6.95
6	250	710	>800	800	250	470	100	400
7	0.15	0.24	0.85	1.31	>1	1	0.085	0.63
8	720	16000	800	>800	450	820	550	8800
9	0.25	1.7	0.29	0.52	0.31	0.88	0.017	0.58
10	140	2200	790	2370	420	820	340	800

[a] nM concentration.

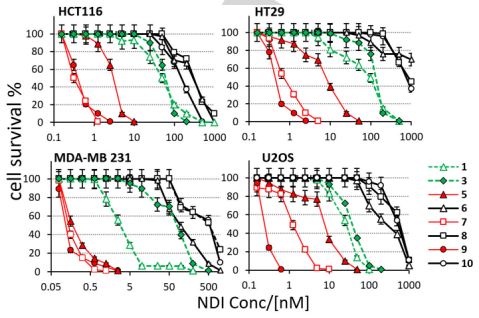

Figure 4. The indicated human tumour cell lines were seeded at clonal density and exposed to different concentrations of compounds for 24 hours. After replacing medium, surviving cells were allowed to grow and form colonies that were stained and counted. Cell survival was calculated as the percentage of colonies in treated compared to untreated conditions. Histograms show the mean values of three independent experiments. Bars indicate means ±SD. Red lines refer to dyads with the long spacer, green lines refer to monomeric NDIs and black lines refer to dyads with the short spacer.

In particular, **7** and **9** were far superior to the monomeric NDIs **1** and **3**, exhibiting sub-nM IC_{50} values for three cell lines (HCT116, HT29, and MDA-MB231), and surprisingly, far superior to the dyads with the shorter butyl linker (**8** and **10**). This superior cytotoxicity of both **7** and **9**, which is a non-dependent cell line feature, is even more striking from the dose dependent cytotoxicity correlations in Figure 4. A similar cytotoxicity behaviour is observed for dyads **5** *vs* **6**, confirming the role played by the linker, with **5** still exhibiting excellent values below 10 nM.

Activation of DNA damage response. To understand the molecular bases of cytotoxicity, the activation of DNA damage response (DDR) was assayed by immunofluorescence analysis against the phosphorylated isoform of H2AX, a hallmark of single and double strand breaks. The cytotoxic activity of all the compounds nicely correlated with DDR induction in transformed fibroblasts, being **9**, **5** and **7** (the compounds with lowest IC_{50}) the most powerful DDR inducers (Figure 5A).

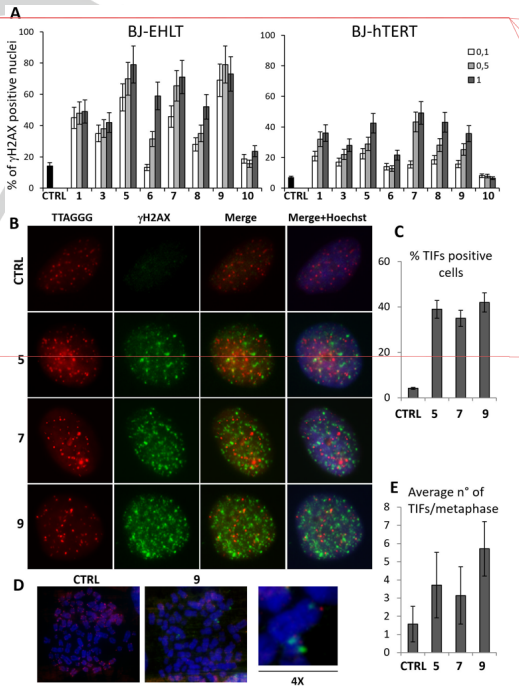

Sara 6/9/y 14:00
Formattato: Non Evidenziato

Sara 6/9/y 14:00
Formattato: Non Evidenziato

Sara 6/9/y 14:00
Formattato: Non Evidenziato

Sara 6/9/y 14:00
Formattato: Tipo di carattere:Non Grassetto

Sara 6/9/y 14:00
Formattato: Tipo di carattere:Non Grassetto

Sara 6/9/y 14:00
Formattato: Tipo di carattere:Non Grassetto

Sara 6/9/y 14:00
Formattato: Tipo di carattere:Non Grassetto

Sara 6/9/y 14:00
Formattato: Tipo di carattere:Non Grassetto

Figure 5. Transformed (BJ-EHLT) and immortalized (BJ-hTERT) human fibroblasts were treated with the dyads at the indicated μM concentrations for 24 hours. Then cells were fixed and processed for indirect immunofluorescence with an anti γH2AX and counterstained with Hoechst. A) Percentage of γH2AX positive nuclei scored at fluorescence microscope (n=200 nuclei/each condition). B) BJ-EHLT cells were treated with 1 μM of the former compounds and processed for Immunofluroescence/FISH with the anti-γH2AX antibody and the Cy3-telo PNA probe (recognizing telomeric DNA). Representative images of co-localization between the two signals, defined as TIFs, are shown (100X magnification). C) Quantification of TIFs positive cells, calculated as the percentage of nuclei displaying more than 4 co-localizing spots. D) BJ-EHLT cells treated with 1 μM of dyad for 24 hours were blocked in metaphase and processed for immunofluroescence/FISH as above, to detect TIFs in metaphase (meta-TIFs). Representative images of meta-TIFs are shown (100X magnification). E) Average number of meta-TIFs s in each metaphase (n=100 metaphases/each condition). Histograms show the mean values of three independent experiments. Bars indicate means ±SD.

Of note, the same compounds were more effective in transformed immortalized fibroblasts (BJ-EHLT) compared to normal ones (BJ-hTERT) (Figure 5A). This evidence suggests a potential higher sensitivity of tumour cells compared to healthy tissues. The three former NDI dyads potently induced also TIFs (telomere's dysfunction induced foci) revealed as co-localization of a rhodamine isothiocyanate derivative (TRITC)-conjugated to a telomeric PNA probe and the γH2AX foci (Figure 5B and C). Not all the DDR foci localized exclusively at telomeres, indicating that other G4 containing regions throughout the genome could be bound. Moreover, **9** induced γH2AX foci persisted after G2 phase (in which the majority of DNA damage is recovered by the HR machinery), being detectable also in metaphase as revealed by the meta-TIFs analysis (Figure 5D and E).

MIC and KIT gene expression. As DDR is observed also outside telomeric regions, we analysed the extra-telomeric effect of compound exposure on G4 containing oncogene promoters. In HCT116, whose proliferative potential relies on an activating kras mutation and an over-expressed c-myc, the expression levels of these two genes was analysed by real-time qPCR assay in treated *vs* untreated cells. Results show that all the compounds were able to inhibit kras expression although to different extent, whereas only **9, 7** and **8** were able to reduce c-myc expression (Figure 6). Therefore, with exception of **9**, which exhibits a remarkable down regulating effect, the expression levels of these two genes does not seem to be directly correlated with the cytotoxic effect in the same cell lines. This suggest that although transcription of G4 bearing oncogene promoters is affected by the dyads, the cytotoxic effects seems to be more related to DDR activation.

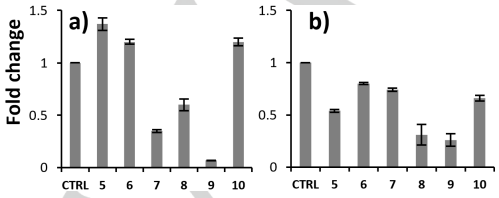

Figure 6. HCT116 cells were treated with the IC_{50} doses of the indicated compound for 24 hours. Then cells were harvested and mRNA was extracted by Trizol and retrotranscribed. cDNA was then processed for real-time qPCR analysis with specific primers towards a) c-myc and b) kras and GAPDH (as control) mRNAs. Histograms represent the fold change of mRNA quantification normalized on GAPDH mRNA as average values of three independent experiments. Bars indicate means ±SD.

NDI dyads inducing DNA aggregation.

In an attempt to get further insight in the behaviour of these dyads, we explored other parameters that can be particularly affected by the length of the linker. In particular, we studied the trend of the absorption baseline, observable in Figure S4, and searched a correlation with their ability to induce aggregation. An ad hoc designed test to see whether the dyads **5**-**8** behave distinctly in inducing aggregation consisted in the preparation of solutions with the dyad in large excess (from 4 to 8 equivalents) over hTel22, registering the absorption spectra and Dynamic Light Scattering (DLS) profiles after filtration. As control, we also checked solutions containing only the dyad. Figure 7 and S7 show the absorption spectra for a large dyad excess and Table S2 reports DLS parameters. In the presence of hTel22, the spectra of the dyads with the longer spacer (**5** and **7**) exhibit features typical for aggregation in particles causing a baseline increase towards the blue side of the spectrum. Moreover, after filtration we lost significant amounts of material, both DNA and dyads. The same loss after filtration was not observed for the dyads with shorter spacer (**6** and **8**). In addition, the solutions with dyads alone did not undergo any loss in material after filtration. The formation of aggregated particles was further confirmed by the DLS data. Reproducible data were obtained only after filtration of the samples. In the case of the dyads **6** and **8** data were not reliable as no particles with diameter discernible by means of DLS were present. On the contrary, dyads **5** and **7** in the presence of hTel22 induced the formation of particles with a diameter of 267 ± 9 nm and 283 ± 8 nm, respectively (Figure S2). The DLS polydispersity parameter with values above 0.3 indicates that likely aggregates of different sizes exist. Thus, the ability to induce a remarkable aggregation of hTel22 seems to be exclusive property of the dyads with the longest $(CH_2)_7$ linker (**5** and **7**) that might allow the dyad to bind different DNA fragments, cross-linking different G4 followed by the formation of aggregates.

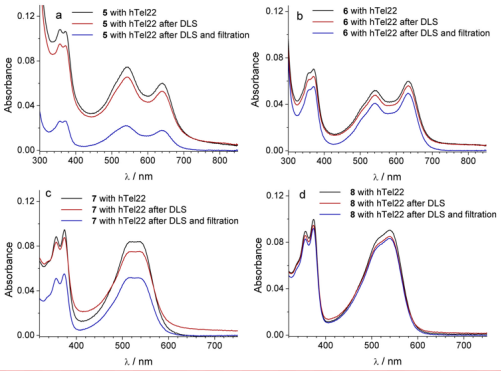

Sara 6/9/y 14:00
Formattato: Non Evidenziato

Sara 6/9/y 14:00
Formattato: Non Evidenziato

Sara 6/9/y 14:00
Formattato: Non Evidenziato

Sara 6/9/y 14:00
Formattato: Non Evidenziato

Sara 6/9/y 14:00
Formattato: Non Evidenziato

Sara 6/9/y 14:00
Formattato: Non Evidenziato

Sara 6/9/y 14:00
Formattato: Non Evidenziato

Sara 6/9/y 14:00
Formattato: Non Evidenziato

Figure 7. Absorption spectra of compounds a) **5**, b) **6**, c) **7** and d) **8** in 8-fold excess with respect to hTel22 (1 μM) before and after DLS and after filtration; 1 cm cuvette.

As hypothesized above in the complexes with 1:2 stoichiometry one or more of the 4 NDIs unit may not be involved in intramolecular-G4 binding, thus having the possibility to interact with a second G4. It is important to underline that the propensity to induce G4 aggregation by the dyads with longer linkers parallels their cytotoxicity, the DDR and TIFs data, rather than their G4-binding properties.

Conclusions

We have prepared new NDI dyads that differentiate in substitution pattern as well as linker length, exploring their DNA binding behavior in solution and their cytotoxicity in selected cell lines. Interestingly, dyads with tetra-substituted NDI units exhibit a fluorescence turn on behavior upon DNA complexation, interesting for their further development in cellular applications. Very good binding constants for G4 DNA were obtained even though the dyads did not exhibit a remarkable over ds DNA. Most importantly, the dyads with the long linker exhibit extremely low IC_{50} values, all below 10 nM on different cancer cell lines. The dyads with shorter linker were much less effective, with IC_{50} values increasing up to 1 μM in some cases. Among the 3 dyads with longer linker, small differences in IC_{50} emerge, suggesting that the length of the linker plays a more important role rather than the substitution pattern. A reason for this may be the ascertained ability of the dyads with the long linker to act as bridge connecting two or more G4 moieties. Even though in cells the condition is not that of dyad excess, we hypothesize the dyads with the longer linker can act as bridge between different telomere clustered G4s, inducing different cytotoxic effects compared to the dyads with the short linker. We have further shown that the dyads are able to induce cellular DDR that is not limited to telomeric regions and is the likely origin of their cytotoxicity. All together, these data are very promising and deserve further exploration in vivo to ascertain the parallelism between G4 aggregation induced by dyads such as **5**, **7** and **9** and cytotoxicity, DDR and TIFs data at a more systemic level.

Experimental Section

Synthesis of the NDIs. We synthesized the reference monomeric NDIs **1-4**, **1-**, **2-Br**, the dyads **5**, **7-9**, **11** and their precursors **17**, **18, 19** and **20** (Scheme 2) according to published procedures. [15], [21], [25]

***N,N'*-Bis-((dimethylamino)propylamino)-2-bromo-6-((amino)butylamino)-1,4-5,8-naphthalenetetracarboxylic bisimide trihydrochloride** (**21**·3HCl)**.**

The crude was purified by preparative HPLC chromatography (method B) and a solution 1M of HCl was added to each chromatographic portion. The solvent was evaporated to dryness under vacuum, obtaining the product as a red solid (yield 50%; m.p. dec.>200°C). ^{1}H-NMR (300 MHz, D_2O): 7.97 (s, 1H), 7.72 (s, 1H), 3.97-3.90 (m, 4H), 3.47 (bs, 2H), 3.13 (bs, 4H), 3.00 (bs, 2H); 2.78 (s, 12H); 1.98-1.96 (m, 4H); 1.78 (bs, 4H). ^{13}C-NMR (75 MHz, D2O): 164.7;161.6; 161.0; 151.0; 136.7; 127.1; 125.6; 121.6; 121.5; 120.7; 119.9; 119.5; 98.2; 55.0; 54.9; 42.6; 42.3; 38.9; 38.0; 37.2; 25.6; 24.2; 22.6; 22.5.

To reduce reaction time and by-products, the following nucleophilic aromatic substitution (S_NAr) was performed using a microwave-assisted protocol. The monomer **18** was dissolved in 5 mL of DMF in a sealed reaction vessel, in the presence of 0.95 equiv. of NDI **17** and 5 equiv. of N,N-diisopropylethylamine. The mixture was stirred and heated in a microwave reactor at 150 °C, 200 psi, 200 W, for 20 min, according to a close vessel protocol. The resulting mixture of crude products was diluted in water, with 0.1% of TFA, and purified by preparative HPLC chromatography (method B). A HCl solution 1M was added to each chromatographic portion and the solvent was evaporated to dryness under vacuum, obtaining the NDI dyads **7** (yield 17%; m.p. dec.>200°C; characterization already published)[25] and **9** (yield 40%; characterization already published).[21]

The same protocol was used in the presence of **19** in order to synthetized the NDI dyads **8** (yield 18%; m.p. dec.>200°C; characterization already published) [25] and **10** (yield 42%; m.p. dec.>200°C).

NDI dyad 10·4HCl. ^{1}H-NMR (300 MHz, D_2O): 8.29-8.27 (m, 2H), 8.03 (d, J=7.90 Hz, 1H), 7.88 (s, 1H), 7.71 (s, 1H), 4.08-4.00 (m, 8H), 3.72 (bs, 2H), 3.64 (bs, 2H), 3.17-3.10 (m, 8H), 2.84 (s, 24H); 2.12-2.05 (m, 12H). ^{13}C-NMR (75 MHz, D2O): 165.3; 165.1; 163.6; 163.4; 163.0; 162.3; 162.1; 161.4; 151.7; 151.3; 137.0; 130.9; 128.2; 126.1; 124.8; 124.5; 121.6; 121.5; 121.3; 120.2; 119.7; 118.1; 98.7; 98.4; 55.2; 55.1; 55.0; 42.7; 42.1; 41.9; 37.5; 36.8; 22.7; 22.6; 22.4.

The NDI dyad **6** has been synthesised in quantitative yield according to a published protocol.[21]

NDI dyad 6·5HCl. ^{1}H-NMR (300 MHz, D_2O): 8.20 (d, J=7.67 Hz, 1H), 7.94 (d, J=7.52 Hz, 1H), 7.71 (s, 1H), 7.66 (s, 1H), 7.54 (s, 1H), 4.07-4.05 (m, 8H), 3.63 (m, 4H), 3.54 (t, J=7.00, 2H), 3.35 (t, J=7.64, 2H), 3.21-3.12 (m, 8H), 2.93 (s, 6H); 2.83 (s, 24H); 2.21 (m, 2H); 2.06-2.02 (m, 12H). ^{13}C-NMR (75 MHz, D2O): 165.5; 165.3; 165.1; 163.9; 163.5; 163.3; 163.2; 151.7; 148.7; 148.1; 130.3; 128.4; 125.9; 124.7; 124.0; 123.7; 121.6; 120.3; 119.9; 119.8; 118.9; 118.2; 116.9; 100.5; 98.4; 55.3; 55.2; 42.7; 41.9;41.7; 39.5; 37.5; 37.0; 36.8; 24.0; 22.7.

The quaternary ammonium salts of all NDI dyads (compounds **11-16**) have been obtained in quantitative yields as iodide.[21]

NDI dyad salt 12. ^{1}H-NMR (300 MHz, D_2O): 8.21 (d, J=7.64 Hz, 1H), 7.96 (d, J=7.57 Hz, 1H), 7.73 (s, 1H), 7.67 (s, 1H), 7.56 (s, 1H), 4.09 (bs, 8H), 3.58 (bs, 6H), 3.40 (bs, 10H), 3.17-3.04 (m, 45H), 2.30 (bs, 4H); 2.10 (bs, 10H). ^{13}C-NMR (75 MHz, D2O): 165.4; 165.2; 165.0; 163.8; 163.5; 163.3; 163.2; 151.7; 148.7; 148.0; 130.3; 128.4;125.9; 124.7; 124.0; 123.7; 121.6; 120.2; 120.0; 119.9; 118.2; 116.9; 101.4; 100.6; 98.5; 64.2; 63.9; 52.8; 42.0; 41.6; 39.3; 37.5; 37.1; 36.9; 23.6; 22.6; 21.3.

NDI dyad salt 14. ^{1}H-NMR (300 MHz, D_2O): 8.39 (s, 1H), 8.09 (d, J=7.84 Hz, 2H), 7.81 (d, J= 7.84 Hz, 2H), 7.65 (s, 1H), 4.08-4.00 (m, 8H), 3.65 (bs, 4H), 3.45 (t, J=7.80, 8H), 3.09 (s, 36H); 2.14 (bs, 12H). ^{13}C-NMR (75 MHz, D2O): 165.07; 163.6; 163.3; 163.2; 162.8; 151.6; 130.8;129.4; 128.1; 125.9; 125.6; 124.6; 124.3; 121.5; 120.2; 119.9; 119.8; 117.8; 98.3; 63.9; 63.7; 52.9;42.2; 37.6; 37.1; 23.7; 21.3.

NDI dyad salt 16. ^{1}H-NMR (300 MHz, D_2O): 8.20-8.18 (m, 2H), 7.94 (d, J=7.83, 1H), 7.78 (s, 1H), 7.64 (s, 1H), 4.10-3.98 (m, 8H), 3.70-3.63 (m, 4H), 3.45 (bs, 8H), 3.09 (s, 36H); 2.14 (bs, 12H). ^{13}C-NMR (75 MHz, D2O): 165.0; 164.9; 163.3; 163.1; 162.8; 161.9; 161.7; 161.1; 151.6; 151.1; 137.0; 130.8; 128.1; 127.4; 126.0; 125.4; 124.6; 124.4; 121.8;

Sara 6/9/y 14:00
Formattato: Non Evidenziato

Unknown
Codice campo modificato

Unknown
Codice campo modificato

Unknown
Codice campo modificato

Unknown
Codice campo modificato

Unknown
Codice campo modificato

Sara 6/9/y 14:00
Formattato: Apice

Unknown
Codice campo modificato

121.5; 120.9; 120.0; 119.8; 117.9; 98.5; 98.3; 63.9; 52.9; 42.4; 38.0; 37.7; 37.2; 37.1; 24.0; 21.3; 21.1.

NDI dyad salt 13. ^{1}H-NMR (300 MHz, D_2O): 7.93 (d, J=7.72, 2H), 7.69 (d, J=7.83, 2H), 7.5 (s, 2H), 4.01 (bs, 8H), 3.43 (bs, 12H), 3.11 (s, 36H); 2.15-2.14 (m, 8H); 1.96 (bs, 4H); 1.78 (bs, 6H). ^{13}C-NMR (75 MHz, D2O): 164.7; 163.0; 162.7; 162.5; 162.2; 161.8; 151.4; 130.7; 127.9; 126.2; 124.5; 124.1; 122.0; 121.4; 119.2; 118.1; 117.6; 114.2; 110.4; 97.7; 63.8; 63.7; 52.9; 43.1; 37.7; 37.1; 28.8; 28.7; 26.8; 21.5; 21.3.

NDI dyad salt 15. 1H-NMR (300 MHz, $(CD_3)_2SO$): 8.53-8.51 (m, 2H), 8.23 (d, J=7.83, 1H) 8.16 (s, 1H), 8.09 (s, 1H), 4.11 (bs, 8H), 3.65 (bs, 4H), 3.49-3.45 (m, 8H), 3.06 (s, 36H); 2.14 (bs, 8H); 1.79 (bs, 4H); 1.54 (bs, 6H). 13C-NMR (75 MHz, D2O): 165.5;165.3; 163; 162.6; 162.5; 161.7; 161.5; 151.8; 151.2; 136.6; 130.8; 128.9; 128.2; 127.9; 127.5; 126; 123.9; 123.3; 122.9; 122.6; 121.2; 118.9; 118.5; 98.9; 98.7; 63.2; 52.2; 42.4; 42.2; 40.7; 40.4; 40.1; 39.8; 39.5; 39.3; 39.0; 38.7; 37.8; 37.4; 37.0; 28.5; 27.8; 26.0; 21.6; 21.4.

Absorption and fluorescence spectra: UV-visible absorption spectra were recorded on a standard Perkin Elmer λ650 spectrophotometer. Fluorescence spectra were measured using 1 nm steps and 0.5-1 s dwell time. Slits were kept as narrow as possible to 4-8 nm in excitation and 4-8 nm in emission. Where necessary a cut-off filter was used. Right angle detection was used. All the measurements were carried out at 295 K in quartz cuvettes with path length of 1 cm. All fluorescence spectra have been obtained for air-equilibrated solutions absorbing less than 0.1 at all wavelengths to avoid inner filter effects and re-absorption of emission. Furthermore, they have been corrected for wavelength dependent response of the monochromator/PMT couple.

Fluorescence lifetimes: Fluorescence decays in solution were measured in air-equilibrated solutions for excitation at 637 nm (Hamamatsu pulsed laser with 1 MHz repetition rate) using a time-correlated single photon counting system (TCSPC) (IBH Consultants Ltd., Glasgow, UK) with a resolution of 55 ps per channel. Photons were detected in right angle configuration at 690 nm with a cut-off filter. Fluorescence decay profiles were analyzed with a least-squares method, using multiexponential decay functions (eq. 2) and deconvolution of the instrumental response function. The software package was provided by IBH Consultants Ltd.

The fitting function used is:

$$I(t) = b + \Sigma_i a_i e(-t/\tau_i) \qquad (2)$$

The fractional intensity and the average fluorescence lifetime are calculated according to the following equations:

$$f_i = a_i\tau_i / \Sigma_j a_j\tau_j \qquad \tau_{av} = \Sigma_j f_j\tau_j$$

Sample Preparation for Titration Studies: For the spectroscopic measurements a 10 mM K^+ phosphate buffer of pH 7.0 was used, with 100 mM KCl. Excess of K^+ mimics physiological conditions of cellular compartments where K^+ is abundant. The DNA stock solution was heated at 90 °C for 15 min and then slowly cooled down to room temperature before use. Concentration of the DNA stock solution was spectrophotometrically determined with 0.1 cm cuvettes. Aliquots of the dyad and DNA solutions dissolved in the same buffer were mixed together to prepare samples of varying molar ratio. Solutions were kept stirring in the dark for ca. 1 hour before starting the measurements. Water was purified by passage through a Millipore MilliQ system (Millipore SpA, Milan, Italy).

Multiwavelength Global analysis: Multiwavelength Global analysis: The best complexation model, the binding constants as well as single spectra of the complexes were determined by means of a multivariate global analysis of multiwavelength fluorescence data, analyzing a set of spectra corresponding to different dyad/DNA mixtures. We used the commercial program ReactLabTM Equilibria (Jplus Consulting Pty Ltd) developed in Matlab®. The procedure is based on singular value decomposition (SVD) and nonlinear regression modelling by the Levenberg-Marquardt method. A matrix is created in Excel with all complete fluorescence spectra, and each spectrum is assigned to a specific DNA concentration. The file is launched from the ReactLabTM Equilibria application. Further parameters introduced before launching the optimization procedure are the ligand concentration, a binding model, approximate binding constants and presence or not of fluorescence of the various species. The analysis proceeds optimizing the single binding constants as well as the spectra of the single species. It eventually affords upon convergence the individual fluorescence spectra of the complexes together with the final binding constants. The former were used to calculate the fluorescence quantum yields of the complexes. The software allows comparison of experimental data and calculated values at single wavelengths to evaluate goodness of the fit. Further statistical outputs include standard deviations for each fitted parameter as well as sum-of-squares and standard deviation for the residuals.

FRET melting assays

All oligonucleotides used in this study were from Sigma-Aldrich (Milan, Italy). For fluorescence melting curves, excess (4x) amounts of the compounds were added to each 5’ -end-FAM (6-carboxyfluorescein) and 3’ -end-TAMRA(6-carboxy-tetramethylrhodamine) 3′ -end-labeled oligonucleotide (0.25 μM) folded in the lithium cacodylate buffer supplemented with potassium (100 mM). After stabilization at 4 °C, samples were processed in a Light Cycler II (Roche, Milan, Italy) or Light Cycler 480 (Roche, Milan, Italy), and the oligonucleotide melting was monitored by observing 6-FAM emission in the temperature range of 30−95 °C with 1 °C/min gradient. Melting profiles were normalized as previously described.[26] T_m was defined as the temperature corresponding to the 0.5 fraction of the normalized fluorescence.

Cell cultures and treatments

HCT116 and HT29 colorectal carcinoma, U2OS osteosarcoma and MDA-MB231 cervix carcinoma cell lines were purchased from ATCC and maintained in D-MEM supplemented with 10% FCS. BJ hTERT and BJ EHLT human fibroblasts were obtained and maintained as previously reported.[27] Compounds **1, 3, 5-10** were dissolved in water. For treatments, working dilutions in culture medium were freshly prepared.

Clonogenic assay

Cells were seeded at clonal density (300-500 cells/well) in six-well plates. After cells had adhered, dyads or vehicle were added to the culture media at concentration ranging from 0,1 to 1000 nM. After 24 hours, medium was replaced and surviving cells were allowed to grow and form colonies for 8-12 days. Colonies were stained with Crystal Violet (Sigma) and manually counted. Survival was calculated as the percentage of surviving clones/seeded cells.

Metaphase spreads.

BJEHLT fibroblasts exposed to 24 hour-treatment with **9** were blocked with demecolcine solution (Sigma) for 2 hours. Metaphases were collected by trypsinization, washed in hypotonic solution (0,075 mM KCl) 10' at 37°C, and then fixed in cold Methanol-Acetic Acid (3:1) solution. Then metaphases were spotted onto glass slices and processed for immunofluorescence/FISH.

Sara 6/9/y 14:00
Formattato: Non Evidenziato

Unknown
Codice campo modificato

Unknown
Codice campo modificato

Immunofluorescence/FISH

Cells were fixed in 2% formaldehyde, permeabilized in 0.25% Triton X100 in PBS for 5 min at room temperature and incubated with the mAb anti-γH2AX (Millipore) followed by the secondary FITC-conjugated Goat anti Mouse antibody (Jackson ImmunoResearch, West Grove, PA, USA). Finally, nuclei were counterstained with Hoechst (Sigma). For combined FISH experiments, after immunofluorescence, samples were re-fixed in 2% formaldehyde and dehydrated by ethanon series. Then slices were hybridized with Cy3 conjugated Telo-PNA probe (Panagene) according to the manufacturer's instruction. Finally, samples were counterstained with Hoechst (Sigma). Fluorescence signals were recorded by using a Leica DMIRE2 microscope equipped with a Leica DFC 350FX camera and elaborated by a Leica FW4000 deconvolution software (Leica, Solms, Germany) at 100X magnification. Fluorescence signals were acquired as above described.

Real time qPCR

HCT116 cells exposed to IC_{50} dose of each compound for 24 hours were collected and RNA was extracted with Trizol reagent (Invitrogen) and converted to complementary DNA with the Tetro Reverse Transcriptase (Bioline, London, UK). Real-time quantitative PCR (qPCR) was performed in triplicate using the 7500 Real Time PCR System (Applied Biosystems, Foster City, CA, USA). The following primers were used: KRAS FWR 5-ACACAAAACAGGCTCAGGACT-3; KRAS REV 5-TTGTCGGATCTCCCTCACCA-3; C-MYC FWR 5-CCATGAGGAGACACCGCC-3; C-MYC REV 5-TCTTGTTCCTCCTCAGEGTCGC-3; GAPDH FWR 5-AGCCTCCCGCTTCGCTCTCT-3; GAPDH-REV 5-GCCAGCATCGCCCCACTTGA-3

The specificity of each PCR products was controlled using the melting curve. The relative gene expression levels were calculated using the 2^(-ΔΔCt) method, where Ct rep-resents the threshold cycle, and GAPDH was used as a reference gene

Confocal Fluorescence Imaging

Fluorescence confocal imaging was performed on an inverted Nikon Ti-E microscope (Nikon Co., Shinjuku, Japan). The confocal fluorescence microscope Nikon A1 is equipped with an Argon ion CW laser and 640 nm CW diode laser. Images were collected using a Nikon Plan Apo VC 60X oil immersion objective with NA 1.40. Filters were set to register the autofluorescence of cells in the 500-550 nm range and the fluorescence of compound **5** in the 663-738 nm range.

Acknowledgements

We gratefully acknowledge the Italian Association for Cancer Research for financial support. [Grant 14708 to M.F.; 16910 to A.B. and 17121 to E.S.].

Keywords: G-quadruplex • dyad ligands • DNA damage • Naphthalene diimide • DNA aggregation

[1] A. T. Phan, V. Kuryavyi, D. J. Patel, *Curr. Opin. Struct. Biol.* **2006**, *16*, 288-298.
[2] M. L. Bochman, K. Paeschke, V. A. Zakian, *Nat. Rev. Genet.* **2012**, *13*, 770-780.
[3] S. Burge, G. N. Parkinson, P. Hazel, A. K. Todd, S. Neidle, *Nucleic Acids Res.* **2006**, *34*, 5402-5415.
[4] J. L. Huppert, S. Balasubramanian, *Nucleic Acids Res.* **2005**, *33*, 2908-2916.
[5] K. A. Lewis, D. S. Wuttke, *Structure* **2012**, *20*, 28-39; Y. Deng, S. S. Chan, S. Chang, *Nat. Rev. Cancer* **2008**, *8*, 450-458.
[6] V. S. Chambers, G. Marsico, J. M. Boutell, M. Di Antonio, G. P. Smith, S. Balasubramanian, *Nature Biotechnology* **2015**, *33*, 877-881.
[7] A. Cammas, S. Millevoi, *Nucleic Acids Res.* **2017**, *45*, 1584-1595; A. Bugaut, S. Balasubramanian, *Nucleic Acids Res.* **2012**, *40*, 4727-4741.
[8] D. Rhodes, H. J. Lipps, *Nucleic Acids Res.* **2015**, *43*, 8627-8637; P. Murat, S. Balasubramanian, *Current Opinion in Genetics & Development* **2014**, *25*, 22-29.
[9] C. Schaffitzel, I. Berger, J. Postberg, J. Hanes, H. J. Lipps, A. Plückthun, *Proc. Natl. Acad. Sci.* **2001**, *98*, 8572-8577.
[10] A. Henderson, Y. Wu, Y. C. Huang, E. A. Chavez, J. Platt, F. B. Johnson, R. M. Brosh, D. Sen, P. M. Lansdorp, *Nucl. Acids Res.* **2014**, *42*, 860-869; A. Siddiqui-Jain, L. H. Hurley, *Nat. Chem.* **2013**, *5*, 153-155.
[11] S. Neidle, *J. Med. Chem.* **2016**, *59*, 5987-6011.
[12] S. Balasubramanian, S. Neidle, *Curr. Opin. Chem. Biol.* **2009**, *13*, 345-353; S. Balasubramanian, L. H. Hurley, S. Neidle, *Nat. Rev. Drug Discov.* **2011**, *10*, 261-275.
[13] V. Pirota, M. Nadai, F. Doria, S. N. Richter, *Molecules* **2019**, *24*.
[14] C. Röger, F. Würthner, *J. Org. Chem.* **2007**, *72*, 8070-8075.
[15] N. Sakai, J. Mareda, E. Vauthey, S. Matile, *Chem Commun* **2010**, *46*, 4225-4237.
[16] F. Doria, M. Nadai, M. Zuffo, R. Perrone, M. Freccero, S. N. Richter, *Chem Commun* **2017**, *53*, 2268-2271.
[17] F. Doria, I. Manet, V. Grande, S. Monti, M. Freccero, *J. Org. Chem.* **2013**, *78*, 8065-8073.
[18] E. Salvati, F. Doria, F. Manoli, C. D'Angelo, A. Biroccio, M. Freccero, I. Manet, *Org Biomol Chem* **2016**, *14*, 7238-7249.
[19] G. W. Collie, R. Promontorio, S. M. Hampel, M. Micco, S. Neidle, G. N. Parkinson, *J. Am. Chem. Soc.* **2012**, *134*, 2723-2731.
[20] F. Cuenca, O. Greciano, M. Gunaratnam, S. Haider, D. Munnur, R. Nanjunda, W. D. Wilson, S. Neidle, *Bioorg. Med. Chem. Lett.* **2008**, *18*, 1668-1673; M. Micco, G. W. Collie, A. G. Dale, S. A. Ohnmacht, I. Pazitna, M. Gunaratnam, A. P. Reszka, S. Neidle, *J. Med. Chem.* **2013**, *56*, 2959-2974; M. Arevalo-Ruiz, F. Doria, E. Belmonte-Reche, A. De Rache, J. Campos-Salinas, R. Lucas, E. Falomir, M. Carda, J. M. Perez-Victoria, J. L. Mergny, M. Freccero, J. C. Morales, *Chem. Eur. J.* **2017**, *23*, 2157-2164.
[21] M. Di Antonio, F. Doria, S. N. Richter, C. Bertipaglia, M. Mella, C. Sissi, M. Palumbo, M. Freccero, *J. Am. Chem. Soc.* **2009**, *131*, 13132-13141; F. Doria, M. Nadai, M. Folini, M. Scalabrin, L. Germani, G. Sattin, M. Mella, M. Palumbo, N. Zaffaroni, D. Fabris, M. Freccero, S. N. Richter, *Chem. Eur. J.* **2013**, *19*, 78-81; M. Nadai, F. Doria, L. Germani, S. N. Richter, M. Freccero, *Chem. Eur. J.* **2015**, *21*, 2330-2334.
[22] M. Micco, G. W. Collie, A. G. Dale, S. A. Ohnmacht, I. Pazitna, M. Gunaratnam, A. P. Reszka, S. Neidle, *J. Med. Chem.* **2013**, *56*, 2959-2974; M. Gunaratnam, M. de la Fuente, S. M. Hampel, A. K. Todd, A. P. Reszka, A. Schatzlein, S. Neidle, *Bioorg. Med. Chem.* **2011**, *19*, 7151-7157.
[23] S. A. Ohnmacht, C. Marchetti, M. Gunaratnam, R. J. Besser, S. M. Haider, G. Di Vita, H. L. Lowe, M. Mellinas-Gomez, S. Diocou, M. Robson, J. Sponer, B. Islam, R. B. Pedley, J. A. Hartley, S. Neidle, *Sci Rep* **2015**, *5*, 11.
[24] F. Doria, A. Oppi, F. Manoli, S. Botti, N. Kandoth, V. Grande, I. Manet, M. Freccero, *Chem. Commun.* **2015**, *51*, 9105-9108.
[25] F. Würthner, S. Ahmed, C. Thalacker, T. Debaerdemaeker, *Chem. Eur. J.* **2002**, *8*, 4742-4750.
[26] J. E. Rogers, S. J. Weiss, L. A. Kelly, *J. Am. Chem. Soc.* **2000**, *122*, 427-436.
[27] S. Bhosale, A. L. Sisson, P. Talukdar, A. Furstenberg, N. Banerji, E. Vauthey, G. Bollot, J. Mareda, C. Roger, F. Wurthner, N. Sakai, S. Matile, *Science* **2006**, *313*, 84-86.

[28] M. Tassinari, G. Cimino-Reale, M. Nadai, F. Doria, E. Butovskaya, M. Recagni, M. Freccero, N. Zaffaroni, S. N. Richter, M. Folini, *J. Med. Chem.* **2018**, *61*, 8625-8638.
[29] P. A. Rachwal, K. R. Fox, *Methods* **2007**, *43*, 291-301.
[30] C. Leonetti, S. Amodei, C. D'Angelo, A. Rizzo, B. Benassi, A. Antonelli, R. Elli, M. F. Stevens, M. D'Incalci, G. Zupi, A. Biroccio, *Mol Pharmacol* **2004**, *66*, 1138-1146.

Entry for the Table of Contents

FULL PAPER

A cytotoxic hug by dyad Nucleic Acid Ligands: Naphthalene diimide dyads exhibit remarkable cytotoxicity (< 10 nM) on different cancer cell lines, which correlates to the length of the linker rather than the structure of the binding moieties

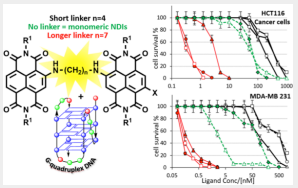

Doria, Filippo; Salvati, Erica; Pompili, Luca; Pirota, Valentina; Manoli, Francesco; Nadai Matteo, Richter N. Sara; Biroccio, Annamaria; Manet, Ilse; Freccero, Mauro**

Page No. – Page No.

G-quadruplex dyad ligands triggering DNA damage response and tumour cell growth inhibition at sub-nM concentration

Sara 6/9/y 14:00
Formattato: Tipo di carattere:Non

Sara 6/9/y 14:00
Formattato: Tipo di carattere:Times New Roman

Sara 6/9/y 14:00
Formattato: Tipo di carattere:Times New Roman

Sara 6/9/y 14:00
Formattato: Tipo di carattere:Grassetto

Sara 6/9/y 14:00
Formattato: Tipo di carattere:Times New Roman

References

Unknown
Codice campo modificato

[1] (a) A. T. Phan, V. Kuryavyi, D. J. Patel, *Curr. Opin. Struct. Biol.* **2006**, *16*, 288-298; (b) J. Choi, T. Majima, *Chem. Soc. Rev.* **2011**, *40*, 5893-5909.

[2] (a) M. L. Bochman, K. Paeschke, V. A. Zakian, *Nat. Rev. Genet.* **2012**, *13*, 770-780; (b) G. W. Collie, G. N. Parkinson, *Chem. Soc. Rev.* **2011**, *40*, 5867-5892.

[3] (a) R. Hansel-Hertsch, D. Beraldi, S. V. Lensing, G. Marsico, K. Zyner, A. Parry, M. Di Antonio, J. Pike, H. Kimura, M. Narita, D. Tannahill, S. Balasubramanian, *Nature Genet.* **2016**, *48*, 1267-1272; (b) R. Hansel-Hertsch, M. Di Antonio, S. Balasubramanian, *Nat. Rev. Mol. Cell Biol.* **2017**, *18*, 279-284; (c) J. L. Huppert, S. Balasubramanian, *Nucleic Acids Research* **2005**, *33*, 2908-2916.

[4] (a) K. A. Lewis, D. S. Wuttke, *Structure* **2012**, *20*, 28-39; (b) Y. Deng, S. S. Chan, S. Chang, *Nat. Rev. Cancer* **2008**, *8*, 450-458.

[5] R. Hansel-Hertsch, J. Spiegel, G. Marsico, D. Tannahill, S. Balasubramanian, *Nat. Protoc.* **2018**, *13*, 551-564.

[6] V. S. Chambers, G. Marsico, J. M. Boutell, M. Di Antonio, G. P. Smith, S. Balasubramanian, *Nature Biotechnology* **2015**, *33*, 877-881.

[7] (a) S. Y. Yang, P. Lejault, S. Chevrier, R. Boidot, A. G. Robertson, J. M. Y. Wong, D. Monchaud, *Nat. Commun.* **2018**, *9*, 11; (b) A. Cammas, S. Millevoi, *Nucleic Acids Research* **2017**, *45*, 1584-1595; (c) C. K. Kwok, G. Marsico, A. B. Sahakyan, V. S. Chambers, S. Balasubramanian, *Nat. Methods* **2016**, *13*, 841-+; (d) A. Bugaut, S. Balasubramanian, *Nucleic Acids Research* **2012**, *40*, 4727-4741.

[8] (a) D. Rhodes, H. J. Lipps, *Nucleic Acids Research* **2015**, *43*, 8627-8637; (b) P. Murat, S. Balasubramanian, *Current Opinion in Genetics & Development* **2014**, *25*, 22-29.

[9] C. Schaffitzel, I. Berger, J. Postberg, J. Hanes, H. J. Lipps, A. PlÃ¼ckthun, *Proceedings of the National Academy of Sciences* **2001**, *98*, 8572-8577.

[10] (a) A. Henderson, Y. Wu, Y. C. Huang, E. A. Chavez, J. Platt, F. B. Johnson, R. M. Brosh, D. Sen, P. M. Lansdorp, *Nucleic Acids Research* **2014**, *42*, 860-869; (b) A. Siddiqui-Jain, L. H. Hurley, *Nat. Chem.* **2013**, *5*, 153-155.

[11] S. Neidle, *Journal of Medicinal Chemistry* **2016**, *59*, 5987-6011.

[12] (a) S. Balasubramanian, S. Neidle, *Curr. Opin. Chem. Biol.* **2009**, *13*, 345-353; (b) S. Balasubramanian, L. H. Hurley, S. Neidle, *Nature Reviews Drug Discovery* **2011**, *10*, 261-275.

[13] V. Pirota, M. Nadai, F. Doria, S. N. Richter, *Molecules (Basel, Switzerland)* **2019**, *24*.
[14] (a) C. Röger, F. Würthner, *The Journal of Organic Chemistry* **2007**, *72*, 8070-8075; (b) N. Sakai, J. Mareda, E. Vauthey, S. Matile, *Chemical communications (Cambridge, England)* **2010**, *46*, 4225-4237; (c) F. Doria, M. Nadai, M. Zuffo, R. Perrone, M. Freccero, S. N. Richter, *Chemical communications (Cambridge, England)* **2017**, *53*, 2268-2271.
[15] F. Doria, I. Manet, V. Grande, S. Monti, M. Freccero, *J Org Chem* **2013**, *78*, 8065-8073.
[16] E. Salvati, F. Doria, F. Manoli, C. D'Angelo, A. Biroccio, M. Freccero, I. Manet, *Organic & biomolecular chemistry* **2016**, *14*, 7238-7249.
[17] (a) G. W. Collie, R. Promontorio, S. M. Hampel, M. Micco, S. Neidle, G. N. Parkinson, *J. Am. Chem. Soc.* **2012**, *134*, 2723-2731; (b) F. Cuenca, O. Greciano, M. Gunaratnam, S. Haider, D. Munnur, R. Nanjunda, W. D. Wilson, S. Neidle, *Bioorg. Med. Chem. Lett.* **2008**, *18*, 1668-1673; (c) M. Micco, G. W. Collie, A. G. Dale, S. A. Ohnmacht, I. Pazitna, M. Gunaratnam, A. P. Reszka, S. Neidle, *J Med Chem* **2013**, *56*, 2959-2974; (d) M. Arevalo-Ruiz, F. Doria, E. Belmonte-Reche, A. De Rache, J. Campos-Salinas, R. Lucas, E. Falomir, M. Carda, J. M. Perez-Victoria, J. L. Mergny, M. Freccero, J. C. Morales, *Chemistry (Weinheim an der Bergstrasse, Germany)* **2017**, *23*, 2157-2164.
[18] (a) M. Di Antonio, F. Doria, S. N. Richter, C. Bertipaglia, M. Mella, C. Sissi, M. Palumbo, M. Freccero, *J Am Chem Soc* **2009**, *131*, 13132-13141; (b) F. Doria, M. Nadai, M. Folini, M. Scalabrin, L. Germani, G. Sattin, M. Mella, M. Palumbo, N. Zaffaroni, D. Fabris, M. Freccero, S. N. Richter, *Chemistry (Weinheim an der Bergstrasse, Germany)* **2013**, *19*, 78-81; (c) M. Nadai, F. Doria, L. Germani, S. N. Richter, M. Freccero, *Chemistry (Weinheim an der Bergstrasse, Germany)* **2015**, *21*, 2330-2334.
[19] (a) M. Micco, G. W. Collie, A. G. Dale, S. A. Ohnmacht, I. Pazitna, M. Gunaratnam, A. P. Reszka, S. Neidle, *J. Med. Chem.* **2013**, *56*, 2959-2974; (b) M. Gunaratnam, M. de la Fuente, S. M. Hampel, A. K. Todd, A. P. Reszka, A. Schatzlein, S. Neidle, *Bioorg. Med. Chem.* **2011**, *19*, 7151-7157.
[20] S. A. Ohnmacht, C. Marchetti, M. Gunaratnam, R. J. Besser, S. M. Haider, G. Di Vita, H. L. Lowe, M. Mellinas-Gomez, S. Diocou, M. Robson, J. Sponer, B. Islam, R. B. Pedley, J. A. Hartley, S. Neidle, *Sci Rep* **2015**, *5*, 11.
[21] F. Doria, A. Oppi, F. Manoli, S. Botti, N. Kandoth, V. Grande, I. Manet, M. Freccero, *Chem. Commun.* **2015**, *51*, 9105-9108.
[22] F. Würthner, S. Ahmed, C. Thalacker, T. Debaerdemaeker, *Chemistry – A European Journal* **2002**, *8*, 4742-4750.
[23] J. E. Rogers, S. J. Weiss, L. A. Kelly, *J. Am. Chem. Soc.* **2000**, *122*, 427-436.
[24] S. Bhosale, A. L. Sisson, P. Talukdar, A. Furstenberg, N. Banerji, E. Vauthey, G. Bollot, J. Mareda, C. Roger, F. Wurthner, N. Sakai, S. Matile, *Science* **2006**, *313*, 84-86.
[25] M. Tassinari, G. Cimino-Reale, M. Nadai, F. Doria, E. Butovskaya, M. Recagni, M. Freccero, N. Zaffaroni, S. N. Richter, M. Folini, *J Med Chem* **2018**, *61*, 8625-8638.
[26] P. A. Rachwal, K. R. Fox, *Methods (San Diego, Calif.)* **2007**, *43*, 291-301.
[27] C. Leonetti, S. Amodei, C. D'Angelo, A. Rizzo, B. Benassi, A. Antonelli, R. Elli, M. F. Stevens, M. D'Incalci, G. Zupi, A. Biroccio, *Molecular pharmacology* **2004**, *66*, 1138-1146.